Article

Deep learning-based quantitative analysis of cerebral microbleeds: Segmentation and classification using CNN

Grace Berin Thomas[1,*], Helen Sulochana Chellakkon[2]

[1] Department of Electronics and Communication Engineering, Ponjesly College of Engineering, Nagercoil, Tamil Nadu 629003, India

[2] Department of Electronics and Communication Engineering, St. Xaviers Catholic College of Engineering, Nagercoil, Tamil Nadu 629003, India

* Corresponding author: Grace Berin Thomas, graceberint@outlook.com

Abstract: Cerebral Microbleeds (CMBs) are among the significant contributors to mortality worldwide and require accurate diagnosis for effective medical intervention. Owing to their wide variability in size, shape, and intensity, manual identification and classification of CMBs in brain imaging remain a complex and error-prone task. This study proposes an automated classification framework for brain MRI-filtered images, categorizing them as either normal or abnormal. The suggested methodology combines a tailored Convolutional Neural Network founded on the ResNet50 architecture, employing a blend of image processing and deep learning strategies. First, a number of preprocessing processes were implemented to increase the MRI pictures quality. One of these steps was the fusion of multi-focus images, which helped to make details more visible. These enhanced images were then processed through a 13-layer CNN architecture specifically designed for effective CMB classification. The strength of the proposed CNN-ResNet50 model was confirmed through validation with two independent datasets. Experiment one used a 10-fold cross-validation procedure, while experiment two split the dataset in half, with 80% used for training and 20% for testing. The model achieved a train-test split accuracy of 98.77% and a cross-validation accuracy of 98.33% while classifying Dataset 1. An accuracy of 92.22% and an accuracy of 93.33% were attained by the model in the two experimental setups for Dataset 2. All investigations used real-world MRI scans. This data set originated from Neyyoor, India's CSI Medical Mission Hospital's International Cancer Center (ICC). The efficacy of the suggested CNN-ResNet50 model was evaluated in comparison to established deep learning models, such as AlexNet and the original ResNet50. Experimental data indicate that our proposed method surpasses both comparative models regarding classification accuracy.

Keywords: cerebral micro bleeding; resnet50 net; convolution neural network

1. Introduction

Small haemorrhages near blood vessels are known as cerebral microbleeds. They are now understood to be crucial diagnostic biomarkers for a variety of cerebral vascular illnesses and cognitive disorders The risk of most unexpected deaths is increased by CMB. A number of internationally analysed logbooks show that CMB is the leading cause of death in society. Prior diagnosis enables it to be de-escalated so that the oncologists can prescribe the appropriate treatment within a set timeframe. MRI scan images are chosen for use in this paper on cerebral micro bleeding. The most sensitive and unique recognition modality that provides cross-sectional images for specific portions of scanned objects is a CAT or MRI scan. The goal of this research is to set up a system that uses MRI pictures as inputs and produces the desired results.

Motivation for this study

Many scientists working in the medical field is adapting contemporary methods for disease prediction. These methods constantly help professionals recognize ailments, implement preventative measures, and streamline treatment planning. The study of CMB diagnosis through MRI of the brain, employing image processing technology, stands out as both a crucial and demanding field of inquiry. However, a significant proportion of people, regardless of age, experience different types of brain haemorrhage. These bleedings can be classified as benign or malignant, with the former being treatable surgically and the latter fatal. The early detection or prediction of CMB will result in the preservation of numerous human lives.

A later stage diagnosis of CMB will put the patient into a comatose or coma, which can occasionally result in death. This encourages researchers to locate and forecast CMB regions in the suspected regions with the first symptoms, and to determine the nature of CMB using MRI scans of the brain. The best technique for predicting the precise location of an area in the brain using an MRI brain picture is determined, along with image processing and segmentation algorithms. The symptoms of headache, changes in vision, trouble speaking or interpreting speech, as well as other complications, are typically used to diagnose CMB while evaluating consecutive scan images.

With the rapid advancement of modern technology, medical imaging applications are evolving continuously to enhance disease diagnosis, analysis, and prevention. As a recent engineering graduate, I am driven to pursue this research with the goal of addressing key challenges that can support the medical community in developing effective strategies for disease prevention. This investigation centers on a significant domain within the field of medicine, utilizing image segmentation and classification methods to identify cerebral microbleeds (CMBs).

2. Literature review

The study on image processing methods and the diagnosis of brain haemorrhage that has been done by various researchers is included in this section. The poll also includes medical information that was used by researchers in their research articles, such as information about various brain disorders or bleeding in various body regions. The application of segmentation, classification, and clustering algorithms for diagnosing medical issues across a variety of domains was also thoroughly covered. The demographic and clinical characteristics of patients with cerebral microbleeds are presented in **Table 1.**

Remove unnecessary noise from the backdrop of the photographs to improve their quality. There are several techniques for preprocessing photos, and each technique has benefits and drawbacks of its own. Some of the components of preprocessing include contrast enhancement, border detection, and the elimination of undesirable noise pixels. Noises in images are eliminated without sacrificing any information in order to aid in the further detection or identification of diseases or affected areas. In this research work, a number of filtering strategies were thoroughly examined in terms of their benefits and drawbacks [1]. They also provided a quick overview of the MRI's properties and noises. During the image acquisition process,

noise distorts the images, lowering their quality. Rician noise with spatially homogeneous noise distribution is the focus of the majority of denoising techniques, [2].

Table 1. Characteristics of cerebral micro bleeding affected patients.

Characteristics		Total patients (%)
Sex	Male	60.71
	Female	40.15
Normal condition		442.02
Ischemic condition		33.69
Hemorrhage condition		24.30
Ischemic condition Age (Years)	Male	Median 61 (22–87)
	Female	Median 55 (31–69)
Hemorrhage condition Age (Years)	Male	Median 39 (27–90)
	Female	Median 45 (10–75)

This program included a number of different preprocessing methods used to find the part of the brain that was bleeding in MRI images. The most important filters that should be used on MRI brain images are noise reduction and smoothing. For this particular database, the results were best for the filter that Perona and Malik had created [3]. Segmentation, Classification, and image extraction are all steps that benefit from well-chosen filters during preprocessing.

This algorithm is evaluated in comparison to existing ones based on its performance metrics. In this context, fuzzy C-means play a vital role. A two-step filtering process was employed in this method. The initial phase employed non-local Principal Component Analysis (PCA) to eliminate noise from the image, while the subsequent phase utilized a non-local mean filter to guide the filtered image. This approach, which is based on the locally imposed bias, fixes images impacted by spatial Rican noise and internally evaluates the total amount of noise in the image [4].

Secondary cerebral microhaemorrhage is typically associated with malignancy and can disseminate to other bodily systems. Each scenario presents the potential for severe and catastrophic outcomes. Using PSO, FCM, EMO, and LSM, we were able to successfully segment digital MRI images for worrisome brain haemorrhage [5].

Concepts of swarm intelligence have garnered significant attention, especially in the realm of PSO. Segmenting MRI images poses a variety of complex challenges. They used PSO and mixed algorithms based on the idea of swarm intelligence in many different areas of their work to show how algorithms can be used in many different situations.

The intensity in homogeneities method of fuzzy logic is used to segment MRI brain data images. The acquisition sequence inhomogeneities imperfection makes a significant contribution to the CMB MRI brain imaging data. The novel algorithm that is being suggested is based on a changed goal function of the FCM algorithm. This changes the values of the voxels by looking at their nearby neighbors. Magnetic resonance imaging (MRI) picture segmentation is a primary use case for this technology because of the substantial impact that salt and pepper noise distortions have on these images. The proposed method's effectiveness and efficiency are illustrated through an evaluation of the algorithm on synthetic data as well as MRI brain images [6].

They go more in-depth with the FCM clustering method in their research. The partition matrix and random initialization are two FCM drawbacks that lead to more erratic clustering outcomes [7]. Although Subtractive Clustering (SC), a different approach, was taken into consideration, it was not known how many clusters there were. To address the limitations of FCM and SC, the authors proposed Subtractive Fuzzy C Means (SFCM), an innovative hybrid technique that integrates FCM and SC. The experimental findings indicate that the SFCM approach provides notably better clustering results compared to the indices of the FCM algorithm [8].

The ABC-FCM algorithm, which combines the FCM and ABC algorithms, is a clustering technique [9]. This innovative method was developed mainly to tackle the limitations associated with the initialization sensitivity of the conventional FCM algorithm, as well as issues related to local optima and cluster centroids [10]. The newly created method took advantage of ABC's capabilities in cluster centres and used these centres as input for the FCM algorithm to enhance the segmentation of MRI brain pictures. Real MRI pictures as well as synthetic brain data are used as input, and the effectiveness of the recently established approach was evaluated [11].

The EMO algorithm's random local search improves and raises the accuracy of the problem solution [12]. In order to solve the population shrinking strategy problem, this research provided a new approach for local search that used and put into practise the pattern search method. The proposed approach was used to solve a few issues, and the outcomes were contrasted with those of the original EMO algorithm.

Few academics have used the EML algorithm to address the Combinatorial Optimization Problem (COP). In order to create a novel hybrid algorithm for determining the best/optimal schedule for the problem, this work aimed to merge the genetic operators with the random key concepts. Upon comparison of the hybrid algorithm's results with those of the standard GA and EMO algorithms, it was evident that the hybrid algorithm yielded superior values [13].

Using image processing techniques, the system that was made worked as a multi-stage diagnostic tool that successfully categorized and identified brain hemorrhage [14]. Combining and changing T1-weighted and T2-weighted magnetic resonance imaging (MRI) images was suggested as a way to get better results. The bleeding zone is extracted from these upgraded MRI images utilizing the watershed segmentation technique and the hybrid skull stripping segmentation process. The bleeding region of the brain can be efficiently segmented using the enhanced watershed segmentation method [15].

The extracted haemorrhage was categorized using SVM to determine if it was benign or cancerous. The created method retrieved the intensity-based features and texture-based features, which were then compared to the actual data. It was fascinating to observe that, on average, the findings produced by the designed system outperformed the ground truth data [16]. Along with the created system, a comparison analysis of two more hybrid classification techniques, such as Morphology + SVM and Watershed + SVM, was carried out. With an accuracy of 94%, the system designed for classifying brain haemorrhage outperformed the other two classification approaches in terms of efficiency [17–19].

Researchers looked at the image segmentation and preprocessing methods they utilized, as well as the medical data they used [20]. The researchers' assessment of

several segmentation algorithms and preprocessing techniques was also covered in this part, along with a brief overview of their benefits and drawbacks [21]. The affected region is analysed with various types of image segmentation algorithms in the section's further discussion of image segmentation algorithms for brain bleeding MRI images. Researchers also looked at the inventive hybrid models they came up with in their thesis for splitting MRI brain imagery into parts. The writers looked into how deep convolutional neural networks can be used to analyze brain pictures [22]. Here, we merely skim the surface of deep convolutional neural networks. nonetheless, it did not mention whether the segmentation.
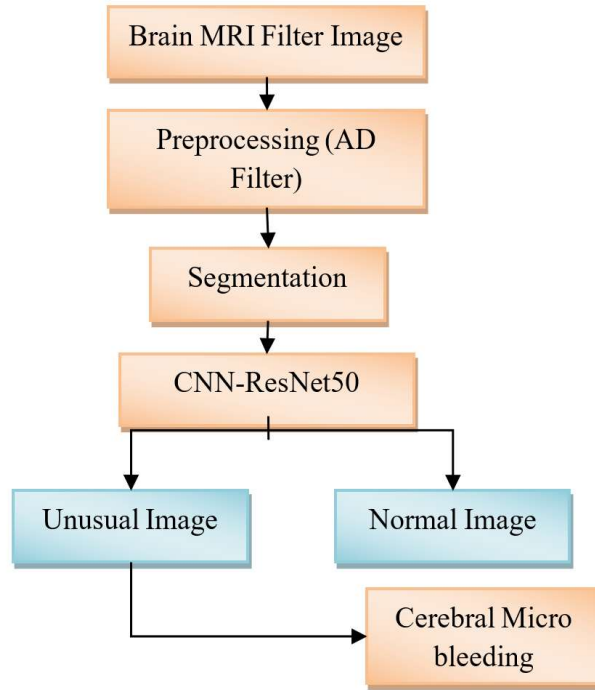
There are two ways to group brain cancer together [9,17]. Most cases of lung cancer are non-small cell lung cancer (NSCLC), which makes up 80% to 90% of cases, and small cell lung cancer (SCLC), which makes up about 10% to 15% of cases. Computer Aided Detection Systems (CAD) are a hotspot for research in medical imaging and diagnostic radiology [8,11,13]. An important part of computer-assisted diagnosis is the ability to categorize picture aspects as normal or abnormal, which allows for the processing of images to detect and eliminate abnormalities [14,18]. A CAD system aids in reducing the incidence of erroneous diagnoses [3,21]. The efficacy of a CAD system is assessed based on accuracy, sensitivity, specificity in diagnosis, speed, and complexity level.

The categorization of brain cancer employs computer-assisted diagnostics via artificial neural networks [1,18]. Area, perimeter, and shape are three fundamental attributes considered in classification. Approximately 90% of the data is categorized in the most severe manner. There are a number of proposed categorization approaches that make use of content-based image retrieval (CBIR) [10,16,20]. A novel system [2] has been designed for the purpose of acquiring open-source lung nodule images. The method extracts images of each individual nodule from the LIDC collection, thereafter determining the Gabor filters, Markov random field properties, and Haralick co-occurrence of the nodule. The distance metrics employed for retrieval are Euclidean, Manhattan, and Chebyshev. The retrieval rate maximum achieved is 88%.

Here is the outline of the paper: Section 2 provides a synopsis of relevant prior work, and Section 3 describes the methodology for categorization that is being considered. Section 4 details the specifics of MRI image datasets, the utilization of nuanced elements, and exploratory findings. Section 5 and 6 of the comprehensive study present a discourse on the exploratory findings.

3. Proposed system

Figure 1 illustrates the proposed paradigm for the detection of Cerebral Microbleed. The procedure commences with input MRI pictures, which undergo preprocessing via an anisotropic filter to enhance image quality. The Anisotropic Diffusion Filter (ADF) is employed to reduce noise while maintaining edge integrity. Subsequently, regions of interest are delineated by deep learning-based bounding box segmentation. This segmentation facilitates the accurate localization of brain microbleeds on MRI imaging. Following DLBB-based segmentation, the segmented CMB image underwent classification. CMB-ResNet 50 CNN was proposed for the categorization of CMB images to ascertain their status as CMB or non-CMB.

Figure 1. Proposed framework for the detection of cerebral micro bleeding.

3.1. Anisotropic diffusion filter (ADF)

The nonlinear anisotropic filter sorts all the pixel values in the window before replacing processing pixels with their median values. The median is determined for each pixel in the image filter mask. The median matrix of size N × M is used to replace the surrounding region of all picture pixels, which are represented by each individual pixel [23]. The new pixel value is more trustworthy and in line with the overall value of the surrounding pixels since it is derived from the median value, which is obtained from nearby pixels. As a result, it displays edge blurring, preserves high frequency information, and preserves image features. The image's median filter's effect grows as the window size does, and it reduces noise more successfully. In order to create the data, AF more correctly eliminates salt and pepper noises. The equation described in 1 can be used to compute median filtering

$$f(x, y) = \text{HAF}_{(s,t)} \in S_{xy}\{g(s,t)\} \tag{1}$$

The sub-image window's coordinates are s × y, the newly computed pixel value is $f(x, y)$, and the window dimensions are N × M. The first steps in preparing MRI brain images are correction and conversion. Next, the picture is transformed into a three-dimensional matrix so that analysis of size, color, and image type may be performed. Implement AF on the MRI image utilizing Equation (2).

$$f(x, y) = \text{AF}_{(s,t)} \in S_{xy}\{g(s,t)\} \tag{2}$$

With N x M window dimensions and s x y sub-image window coordinates, the computed pixel value is denoted as $f(x, y)$. Keep all relevant details, such as execution time, memory size, and pixel variance, together with the final photos for future investigation.

ADF improves MRI preprocessing by lowering noise while maintaining crucial structural elements, like edges and minute anatomical characteristics that are essential for CMB detection [24]. ADF selectively smoothes uniform regions while preserving high-frequency information, in contrast to conventional smoothing techniques that blur edges. Its median-based methodology also successfully reduces salt-and-pepper noise. In comparison to previous preprocessing methods, this harmony between noise reduction and feature preservation enhances the quality of input images, enabling the CNN-ResNet50 model to extract more trustworthy features and eventually reach greater classification accuracy.

3.2. Deep learning bounding box segmentation

The goal of segmentations is to define or recognize various tissues by differentiating the intensity values of the pixels that make up the image. When working with a 2D slice or voxel, it is processed as a 2D image, whereas in the case of 3D volume data, it utilizes the essential MRI values. For various medical analyses, including surgical planning, clinical diagnosis, locating areas of pathology, and analyzing anatomical features, segmenting an MRI brain image is a crucial first step. Due to disturbances and overlapping ranges of intensity values, segmenting the brain is a difficult operation. In the preparation phase, the implementation of the Deep Learning the Bounding Box (DLBB) method initiates by determining the quantity of clusters to be utilized. First, the cluster centers are established, followed by the computation of the partition matrix elements. Based on these values, the cluster center is then updated. Steps involving the calculation of the partition matrix and the cluster center are repeated iteratively until the termination condition is satisfied.

The DLBB algorithm's principal objective, when applied to these input MRI brain pictures, is to extract the intensity values that correspond to the CMB affected region. It iteratively chooses pixel values at random in accordance with the DLBB algorithm's definitions and functions DLBB's objective function and membership function, represented by the U matrix, form its foundation. Only the integers 0 and 1 are used by the hard c-means membership function, however each cluster's membership data points are kept between 0 and 1. Key parameters are in the DLBB algorithm's objective function output arguments. Each row of the Center parameter's matrix of final cluster centers represents the image's pixel cluster centers. There is one more fuzzy division matrix, which is called U. which represents the output image's segmented regions [25]. Finally, the Obj-fuc parameter records the objective function values produced during each picture pixel iteration, revealing clustering convergence and performance.

The Image set X, is taken as

$$X = (X_i)_{i=1}^{N} \tag{3}$$

In the DLBB segmentation process, the initial membership matrix, denoted as *nU0*, is initialized randomly. During each iteration, the algorithm updates the membership values, which lie between 0 and 1, representing the degree of association of each data point with the respective clusters. Unlike hard c-means clustering, which assigns membership values strictly as 0 or 1 (indicating exclusive membership to one cluster), the DLBB algorithm allows for soft clustering, in this context, each data point

may have a degree of association with several clusters, influenced by its proximity and similarity to them.

$$J^1(u,v) = \sum_{i=1}^{c} \sum_{j=1}^{n} u_{ij}^m \|X_j - V_i\|^2 \tag{4}$$

The equation requires the membership matrix U, cluster center matrix V, N pixel points, C clusters, j^{th} measured pixel point X, and cluster center i. Implement the equation

$$J^1(u,v) = \sum_{i=1}^{c} \sum_{j=1}^{n} u_{ij}^m \|X_j - V_k\|^2 \tag{5}$$

u represents the membership value of j X in relation to the cluster i.

$$u_{ij} = \frac{1}{\sum_{k=1}^{c} (\|X_j - V_i\| / \|X_j - V_k\|)^{2/(m-1)}} \tag{6}$$

When the image is set to clusters, each pixel point is taken in account and involved in the cluster process. n is the numbers of clusters with default starting value which is greater than one. This flexibility enhances the accuracy and adaptability of segmentation, particularly in complex medical images used for cerebral microbleed detection.

The DLBB segmentation approach described here is an adaptation of fuzzy clustering methods rather than a completely novel algorithm. Its foundation lies in the principles of fuzzy c-means clustering, where pixel intensities are assigned membership values between 0 and 1, allowing for soft clustering and better handling of overlapping intensity ranges common in medical images. However, the DLBB method extends this concept by incorporating a bounding-box–based framework tailored for medical image segmentation, specifically targeting cerebral microbleed regions. By iteratively updating cluster centers and membership values through the objective function and introducing bounding constraints to localize pathological regions [26], DLBB enhances the accuracy and convergence stability compared to conventional fuzzy clustering. Thus, while it builds upon established fuzzy clustering theory, its application in MRI-based CMB detection and the integration of bounding-box constraints represent a specialized adaptation rather than a wholly new clustering paradigm.

3.3. Image classification resnet50 network

The classification model is fed the cerebral microbleed (CMB) pictures after the preprocessing step. A training set of CMB pictures is used as an example to run a ResNet-based Convolutional Neural Network (CNN) on the already-processed dataset. Once the model has been learned, the testing set is categorized. The grayscale MRI pictures of brain strokes are represented by resizing the input images to dimensions of $512 \times 512 \times 1$. There is a total of four layers in the suggested ResNet CNN design: two convolutional and two densely linked. The model's small size and efficient network architecture allow it to detect CMBs with good classification accuracy using very little computational resources.

Layer of Convolutional Neural Network Classifier Convolutional layers preserve spatial structure, in contrast to more conventional fully connected neural network layers, which is a key distinction between the two. As an example, the 32 × 32 s× 3 image keeps its unique 2D structure instead of being shrunk to a one-dimensional vector of 3072 objects. The convolutional channel not only safeguards basic properties but also transforms the input into an additional tensor called an actuation map. A low-dimensional vector space rich with elements can be created using conventional fully associated systems by stacking convolutional layers, thus reducing the dimensionality of the spatial information. This allows for the re-convolution of maps without sacrificing auxiliary data. One such approach to dealing with areas with limited input volume is the CNN Classifier's Pooling Layer. The pooling layer runs collections over areas instead of duplicating using channels with prepared loads. Aggregation usually takes place near the area limit, which is also the name of the maximal pooling layer. Here are a few key layers that ResNet CNN has utilized during its training and testing:

Convolution: The image layer convolves a filter of identical depth to the image for each element, thereby extracting features from it.

ReLU: After every convolutional layer, this layer is added to threshold all the input values. As shown below, any negative value in this layer is set to zero.

$$f(x) = \begin{cases} x & x \geq 0 \\ 0 & x < 0 \end{cases} \tag{7}$$

Maximum Pooling: This layer selects the finest feature response from nearby neighborhoods through down-sampling. The result is featuring maps that are smaller. Improving translation invariance is another purpose for it.

Dropout: avoids overfitting in networks by regularization.

Fully Connected: This layer performs multiplication of the input by a weight matrix and adds a bias vector. The SoftMax layer normalizes the output within the range of [0, 1].

The equation is expressed in Cartesian coordinates as, in Equation (3),

$$(x - a)^2 + (y - b)^2 = r^2 \tag{8}$$

The most potent hidden layer in CMB-ResNet CNN enables the automatic detection and categorization of cancerous cells from extensive microscopic datasets. A picture's fitness value can be calculated using Equation (4),

$$f = \frac{W - K + 2P}{S} + 1 \tag{9}$$

W represents the input volume, K the kernel field, S the pixels, and P the image's padded values. Equation gives P

$$P = (K - 1)/2 \tag{10}$$

ResNet50 was selected for this work because of its shown ability to balance depth, computational efficiency, and robust feature extraction, which makes it especially well-suited for applications involving medical picture analysis, like CMB categorization. ResNet50, in contrast to some more recent architectures, uses residual connections to address the vanishing gradient issue, enabling deeper networks without compromising training stability. This is essential for capturing the minute changes in

CMBs' size, shape, and intensity that are shown in MRI images. Larger datasets and more processing power are frequently needed to get optimal performance, even when designs like EfficientNet, DenseNet, or Vision Transformers provide benefits like improved feature reuse, parameter efficiency, or attention-based global context modeling. ResNet50 offered a dependable and well-understood framework that could achieve high classification accuracy with reasonable training complexity, guaranteeing both robustness and reproducibility of results based on real-world MRI scans from a single medical center.

4. Implementation details and performance measures

We evaluated the proposed technique on our 64-bit workstation, featuring a 3.70 GHz Intel(R) Xeon(R) CPU E5-1630 v4, 32 GB RAM, and a Quadro K1200 CUDA device, utilizing MATLAB 2018b.Two datasets were used for the testing. For 10-fold cross-validation, we conducted a different study in which we divided the image collection into 80% preparation and 20% testing. Then the applied image underwent pretreatment to generate higher-quality test images for classification. Next, the training dataset is used to develop the suggested 13-layer ResNet CNN demonstration; next, the testing dataset is used to generate the classification results. The following performance measures such as, genuine positive rate (TPR), incorrect positive rate (FPR), F-measure, and exactness (ACC) are the assessment measures to determine whether our technique was effective. These are determined by:

$$Precision = \frac{TP}{TP + FP} \tag{11}$$

$$TPT = \frac{TP}{TP + FN} \tag{12}$$

$$FPR = \frac{FP}{FP + TN} \tag{13}$$

$$F_{Measure} = 2\frac{Precision \; x \; TPR}{Precision \; x \; TPR} \tag{14}$$

$$ACC = \frac{TP + TN}{TP + FP + TN + FN} \tag{15}$$

where the values for false negative (FN), false positive (FP), true negative (TN), and true positive (TP) are corresponding.

Epochs: The number of times the model runs across the whole training dataset is determined by the number of epochs. Underfitting, in which the model is unable to learn the intricate patterns that differentiate normal from aberrant MRI scans, can occur when too few epochs are selected. On the other hand, overfitting may result from using too many epochs, particularly considering the datasets' moderate size. Epochs were empirically chosen for this investigation by tracking the convergence of training and validation losses to make sure the model learned enough without overfitting.
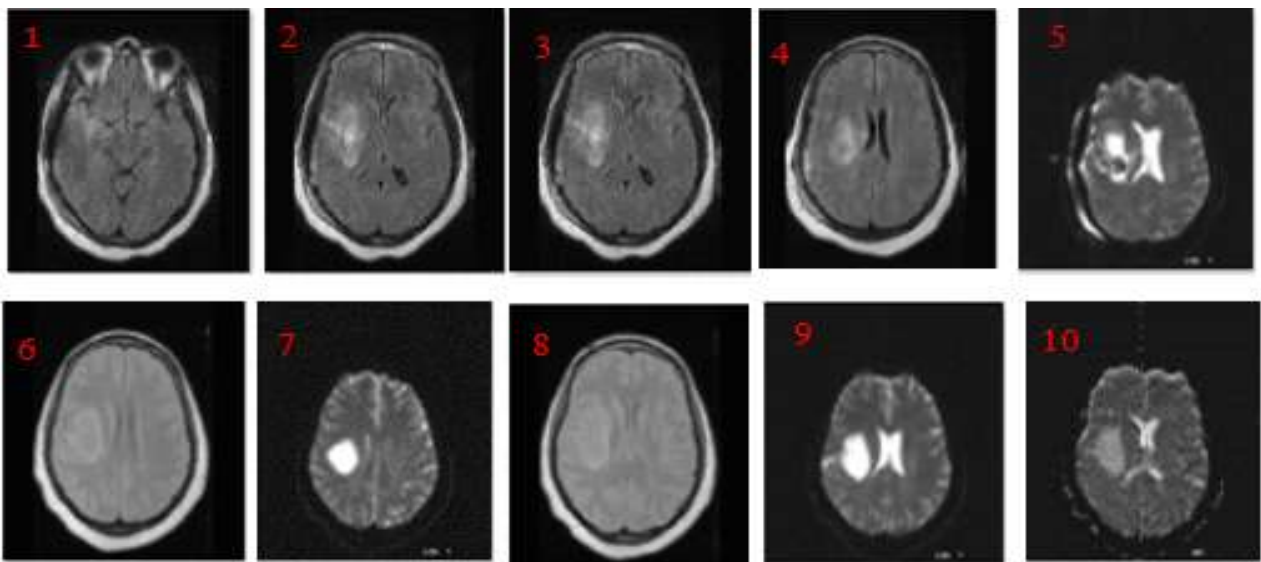
Learning Rate: During training, the step size of weight updates is controlled by the learning rate. While a very low learning rate slows down convergence and

lengthens training time, a high rate may cause the model to overshoot ideal minima. To ensure that the model correctly caught minor features in CMBs, the study used a learning rate schedule or adjusted the learning rate through experimentation to balance fast convergence with stable training.

Batch Size: The number of data processed before the model updates its weights depends on the batch size. Although they require additional training time, smaller batch sizes provide more detailed weight updates and can enhance generalization. Although larger batch sizes shorten training times, they may also make it harder for the model to generalize to new data. The batch size in this study was chosen to take into consideration the memory limitations of processing high-resolution MRI images while balancing computational efficiency and model generalization.
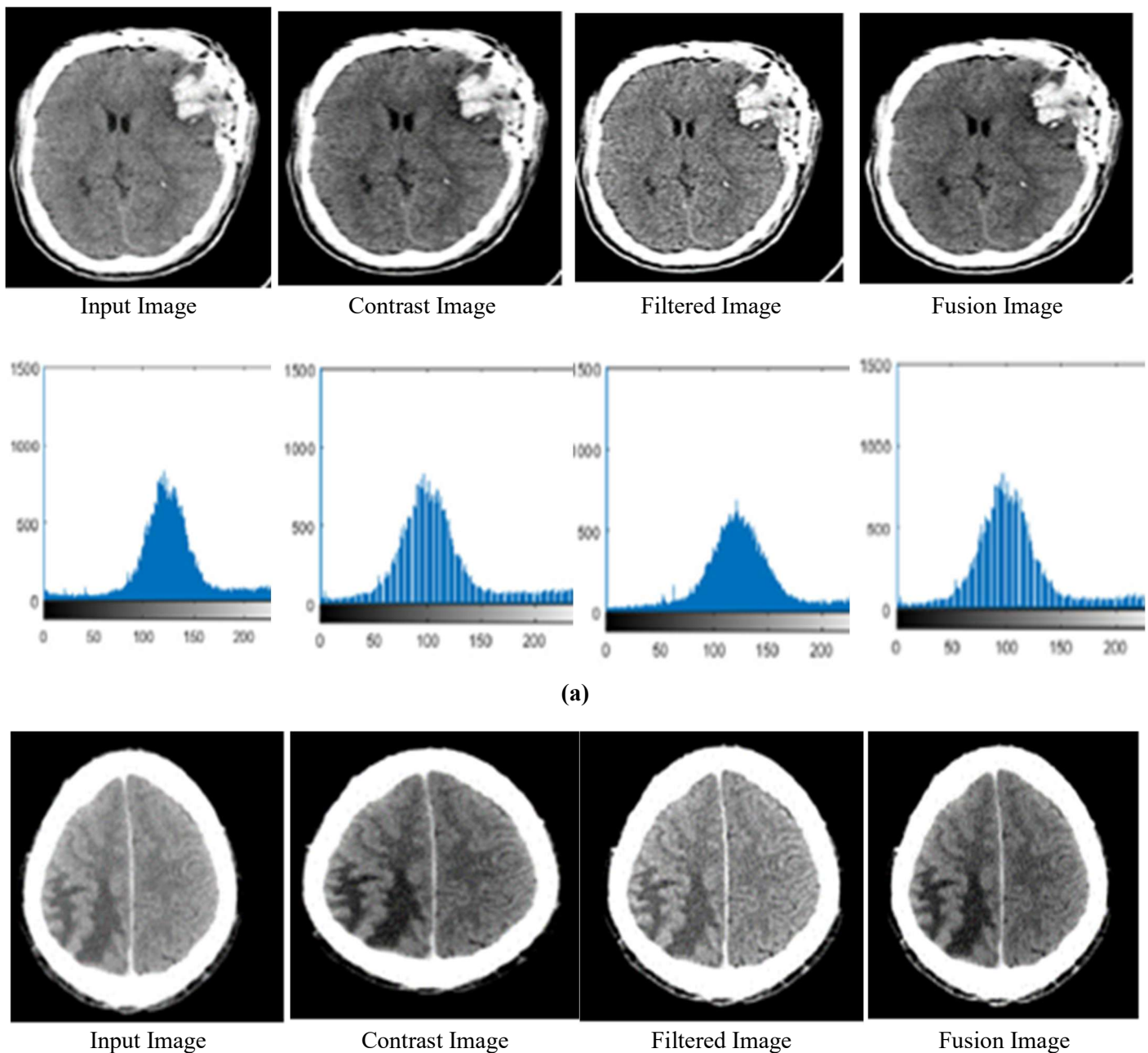
5. Result and discussion

A crucial and substantial obstacle in segmentation is the identification and detection of cerebral microbleeding. Rapid, accurate diagnosis of picture qualities for medical applications is challenging. The DLBB method is applicable for analyzing data from brain MRI scans to identify hemorrhage. Initialization occurs during preprocessing, further steps include segmentation, and lastly validation. The ResNet model was trained on the picture dataset for 30 epochs with a learning rate of 0.001, utilizing the SGDM technique for optimization. Employing the training model for image categorization on the test dataset. Our suggested AlexNet network uses 128 samples per batch, while ResNet50 uses 12 samples per batch. **Figure 2** illustrates representative brain MRI images showing cerebral micro bleeding patterns used in this study.
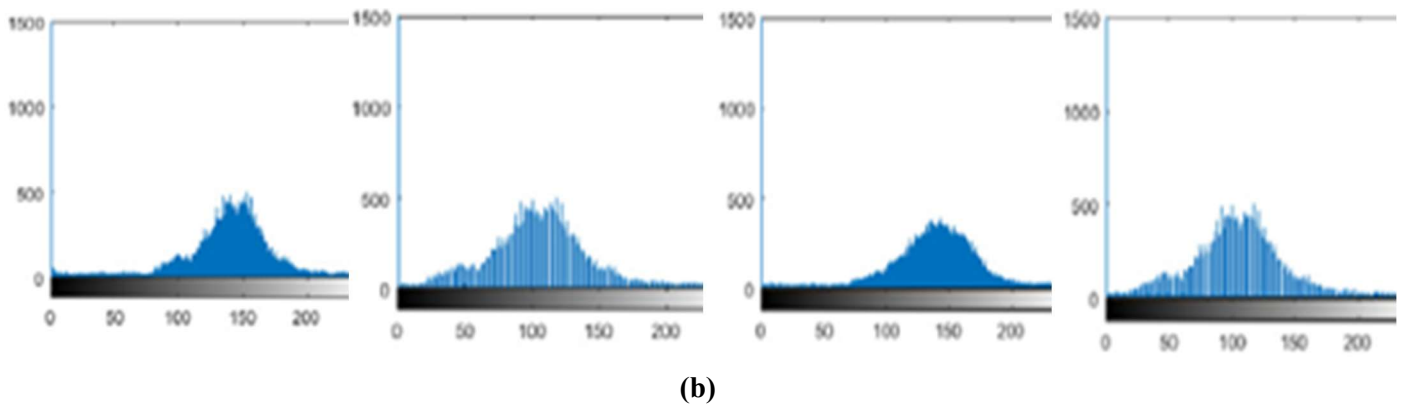

Figure 2. Sample brain bleeding images.

The CSI restorative Mission Clinic at the Worldwide Cancer Center (ICC) in Neyyoor, India, provided the images of brain bleeding used in this research. We gathered MRI scan images, images of healthy and unhealthy CMBs, and images from a standard MRI. All of the images in the collection are DICOM files generated by a 64-Slice SOMATOM MRI Scanner. Image slices are 512 by 512 pixels, and voxels

are 0.412 by 0.412 by 5.1 millimeters. All cerebral stroke images are produced with the same scanning parameters—400 mAs exposure, 120 kV tube voltage, and 2.4 mm to 4.8 mm slice thickness. The 900 pictures represent 74 patients, with 300 MRI photos each group. The exclusion criteria excluded MRI scans with significant motion artifacts, insufficient data, or other neurological problems, while the inclusion criteria included scans with clear structural visibility and a verified diagnosis or suspicion of CMBs. By taking these precautions, the dataset was guaranteed to be methodologically sound and therapeutically appropriate for assessing the suggested deep learning models. The preprocessing pipeline and corresponding histogram analysis of MRI images are presented in **Figure 3**.

| Input Image | Contrast Image | Filtered Image | Fusion Image |

(a)

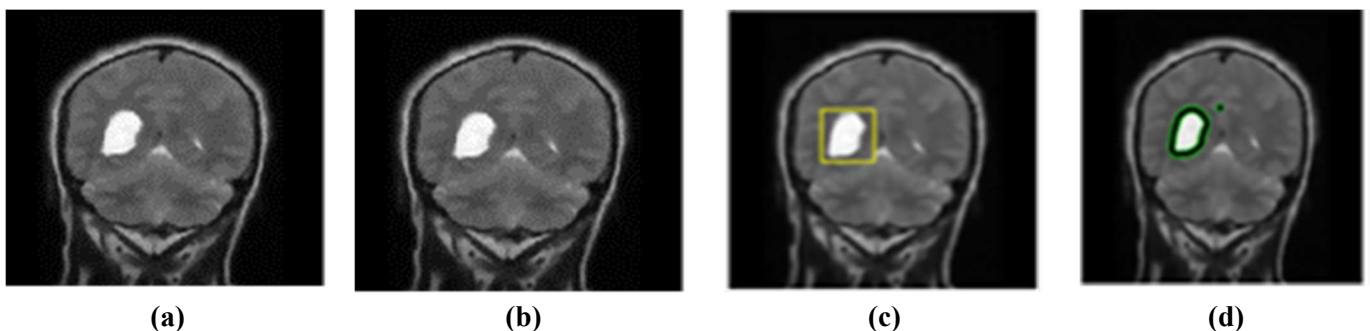| Input Image | Contrast Image | Filtered Image | Fusion Image |

(b)

Figure 3. Image preprocessing pipeline and corresponding histogram analysis for brain MRI images: **(a)** preprocessing stages applied to a normal MRI image, including the input image, contrast-enhanced image, anisotropically filtered image, and fused image; **(b)** preprocessing stages applied to an abnormal MRI image with cerebral microbleeds, showing the same sequence of input, contrast enhancement, filtering, and image fusion.

The dataset was divided at the patient level instead of the image level to prevent patient-level data leakage and guarantee the validity of the experimental results. This means that every MRI scan of a single patient was only ever included in the training or testing sets, never both. This tactic stopped the algorithm from inadvertently picking up patient-specific characteristics that might have inflated performance indicators. A 10-fold cross-validation method was employed for Dataset 1, which was split up into ten patient-level folds. In each iteration, nine folds were utilized for training and one-fold was used for testing. An 80:20 split was used in Dataset 2, where 20% of patients were assigned to the testing set and 80% to the training set. This made sure that the evaluation findings accurately represented the model's capacity to generalize to patient data that had not yet been encountered. The experimental segmentation results for a benign cerebral microbleed case are illustrated in **Figure 4**. The experimental results for a malignant cerebral microbleed are shown in **Figure 5**. A comparative evaluation of different image preprocessing techniques based on PSNR, SSIM, and MSE metrics is presented in **Table 2**.
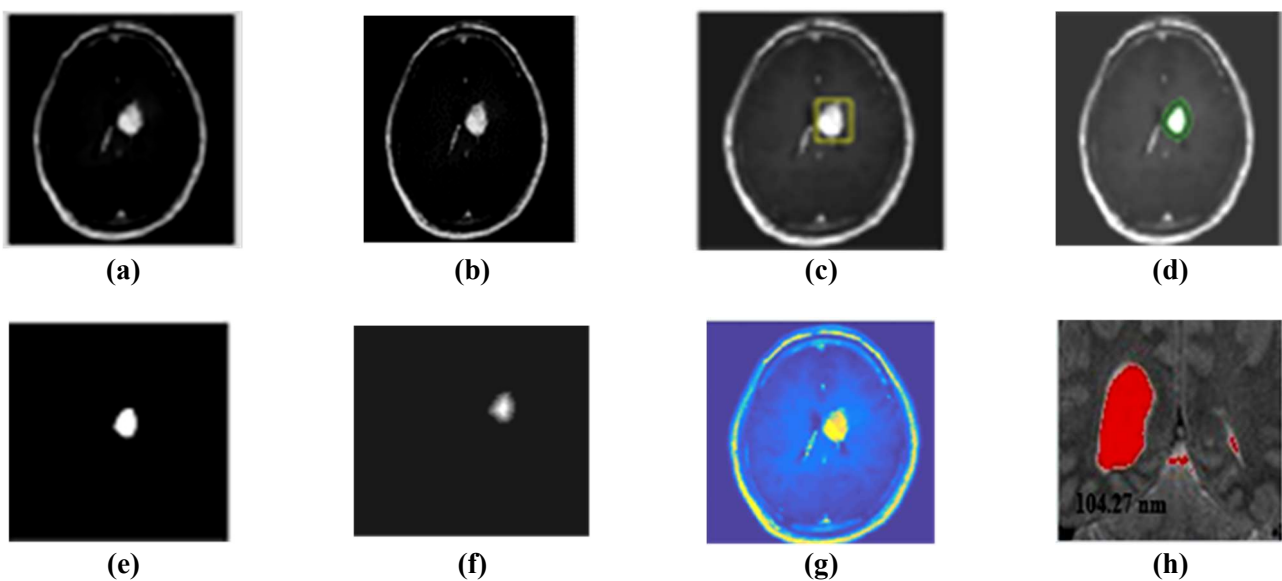
Table 2. Comparative evaluation of pre-processing techniques.

Evaluation metric	Unsharp masking	Bilateral filtering	Anisotropic diffusion
PSNR (dB)	28.54	28.61	37.98
SSIM	0.8462	0.8251	0.9258
MSE	0.0048	0.0019	0.00058

(a)   **(b)**   **(c)**   **(d)**

Figure 4. Experimental result of benign cerebral micro bleeding image. **(a)** brain affected by CMB, **(b)** anisotropic filter image, **(c)** locating seed box image, **(d)** CMB region marked image, **(e)** segmented bleeding region image, **(f)** DLBB segmented image, **(g)** DLBB segmentation coloring Image, **(h)** area red marked image.

Figure 5. Experimental result of malignant cerebral micro bleeding. **(a)** brain affected by CMB, **(b)** anisotropic filter image, **(c)** locating seed box image, **(d)** CMB region marked image, **(e)** segmented CMB region image, **(f)** DLBB segmented image, **(g)** DLBB segmentation coloring Image, **(h)** area red marked image.

Table 3 shows how well four deep learning models—P-CNN, AlexNet, P-CNN-WP, and ResNet50 performed on a dataset with an 80% training and 20% testing split. Each model's precision, accuracy, F1-score, recall (TPR), and false positive rate (FPR) are presented. With an overall accuracy of 98.36%, a precision of 0.9993, a recall of 0.9923, an F1-score of 0.98, and a low false positive rate of 0.01668, ResNet50 outperformed the other models. With accuracies of 95.5% and 98.5%, respectively, the AlexNet and P-CNN-WP models again demonstrated strong performance; however, ResNet50 surpassed them in both recall and FPR, demonstrating a stronger capacity to accurately identify pictures while reducing misclassification. Deeper architectures, such as ResNet50, are more successful for this classification job, as evidenced by the baseline P-CNN model's lowest precision and accuracy.

The classification performance of the first picture dataset using four deep learning models (P-CNN, AlexNet, P-CNN-WP, and ResNet50) following 10 rounds of cross-validation is summarized in the **Table 4**. Precision, recall (true positive rate), false positive rate (FPR), F1-score, and total accuracy are used to gauge each model's efficacy. With a precision of 0.967, recall of 0.9825, FPR of 0.014, F1-score of 0.988,

and accuracy of 98.648%, ResNet50 outperformed the other models, demonstrating exceptional dependability in accurately identifying images. AlexNet and P-CNN performed marginally worse, with accuracies of 95.34% and 96.34%, respectively, whereas P-CNN-WP likewise performed well, reaching almost 98% accuracy. Overall, the findings imply that ResNet50 offers this dataset the best reliable and well-balanced classification performance.

Table 3. Precision in picture classification using a 20% test set and an 80% training set.

Model	Precision	Recall (TPR)	False Positive Rate (FPR)	F1-Score	Accuracy (%)
P-CNN	0.9014	0.8998	0.101	0.898	89.9
AlexNet	0.9761	0.984	0.023	0.98	95.5
P-CNN-WP	0.9843	0.965	0.027	0.98	98.5
ResNet50	0.9993	0.9923	0.01668	0.98	98.36

Table 4. The results of the first image dataset's classification accuracy after ten rounds of cross-validation.

Model	Precision	Recall (TPR)	False Positive Rate (FPR)	F1-Score	Accuracy (%)
P-CNN	0.954	0.951	0.042	0.952	96.34
AlexNet	0.982	0.975	0.021	0.98	95.34
P-CNN-WP	0.96	0.965	0.018	0.968	97.98
ResNet50	0.967	0.9825	0.014	0.988	98.648

Table 5 shows that compared to P-CNN's 91.40% average classification accuracy, AlexNet's is just 91.20%. In contrast, our ResNet50 achieves an accuracy of 92.80% when used for image classification; but, when we forego image preparation and refer to this approach as P_CNN_WP (meaning "without preprocessing"), the accuracy drops to 91.59%. But when compared to others, ResNet50 produces superior classification results. Analyzing the proposed method's essential components on the MATLAB (R2018b) validation set. ER stands for the enhancing region. The entire region, according to WR. (Core for Brain Bleeding). To test the efficacy of dilated convolution, we conduct independent experiments with different values of the parameters: dilated parameter = 3, kernel size = 3, dilated parameter = 2, kernel size = 5, dilated parameter = 3, kernel size = 5, and finally, no dilated convolution at all. The segmentation performance under various convolutional and architectural settings is reported in **Table 6.**
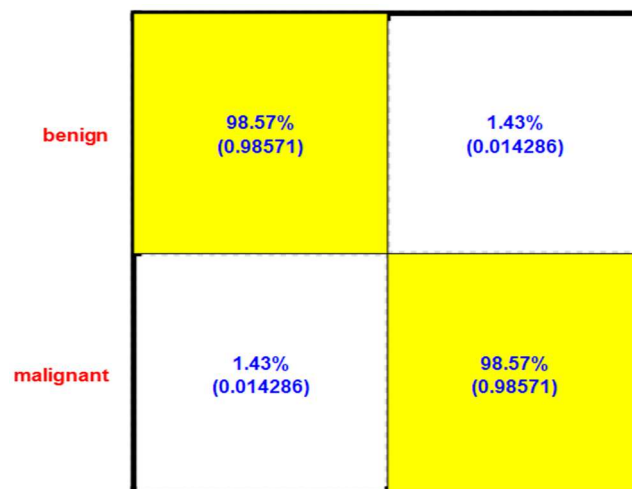
Table 5. Performance metrics of CNN-based models on dataset 2 (80% training,20% testing).

Model	Precision	Recall (TPR)	False Positive Rate (FPR)	F1-Score	Accuracy (%)
P-CNN	0.865	0.872	0.065	0.868	87.25
AlexNet	0.908	0.910	0.045	0.909	91.20
P-CNN-WP	0.915	0.917	0.048	0.916	91.40
ResNet50	0.928	0.926	0.037	0.927	92.80

Table 6. Convolution layer metrics.

Method		Dice			Sensitivity			Specificity		
		ER	WR	BBC	ER	WR	BBC	ER	WR	BBC
Proposed	Brain TS 2019	0.7611	0.8899	0.7787	0.767	0.8831	0.7624	0.9951	0.9981	0.9968
	Brain TS 2018	0.7712	0.8998	0.7946	0.7687	0.9039	0.7509	0.9983	0.9948	0.9984
Dilated convolution	No dilated convolution	0.7020	0.8802	0.7533	0.7369	0.9038	0.7444	0.9981	0.9923	0.9970
	Dilation-3 and kernel-3	0.7619	0.8955	0.7787	0.7680	0.8858	0.7508	0.9982	0.9951	0.9973
	Dilation-4 and kernel-3	0.7309	0.8589	0.7825	0.7589	0.8686	0.7693	0.9981	0.9927	0.9972
	Dilation-2 and kernel-5	0.7577	0.8972	0.7895	0.7847	0.8861	0.7562	0.9979	0.9979	0.9977
Pooling	No pooling	0.5378	0.6682	0.5564	0.6216	0.5630	0.5973	0.9964	0.9964	0.9904
	Average pooling	0.7525	0.8945	0.7763	0.7521	0.8812	0.7440	0.9984	0.9954	0.9978
Kernel size	Kernel size of 5	0.6906	0.8881	0.7268	0.7478	0.8982	0.6912	0.9979	0.9937	0.998
	Kernel size of 7	0.6731	0.8923	0.70565	0.6683	0.8860	0.6887	0.9989	0.9952	0.9961
Activation function	ReLU	0.7266	0.8834	0.7602	0.7461	0.8572	0.7362	0.9983	0.9961	0.9973
	Leaky ReLU	0.7285	0.8869	0.7601	0.7444	0.9007	0.7466	0.9983	0.9935	0.9969
No pre-processing		0.6229	0.8247	0.5524	0.5927	0.8488	0.4743	0.9991	0.9911	0.9992
Using one pathway		0.7288	0.8890	0.7401	0.7744	0.8876	0.6984	0.9978	0.995	0.9984

The output class confusion matrix and its graphic representation. The green boxes represent the actual positive values in this matrix, while the red boxes represent the actual negative values. It is possible to find the most accurate feature amalgamations from the table. An improved accuracy of 98.57% is the end effect of this. The confusion matrix illustrating the classification outcomes of the CNN classifier is presented in **Figure 6**.

Figure 6. Confusion matrix of CNN classifier.

The training time comparison of different CNN models on Dataset 1 is presented in **Table 7**. The corresponding training time results for Dataset 2 are summarized in **Table 8**. Compared to 1-fold training, 10-fold cross-validation takes ten times longer. Recommended methods ResNet50 and P_CNN train and categorize faster than competing methods due to fewer network layers. Since network layer count and input image size are directly related to training duration.

Table 7. Training time comparison of CNN models on dataset 1(80% split and 1-fold training).

Model	Training time (80% split)	Training time (1-fold)
P-CNN	1 min 42sec	2 min 17sec
AlexNet	21 min 44 sec	25 min 25 sec
P-CNN-WP	2 min 49 sec	4 min 01 sec
ResNet50	2 min 45 sec	3 min 25sec

Table 8. Time it took to train the classification model on 80% of the picture dataset and one-fold of it.

Model	Training time (80% split)	Training time (1-fold)
P-CNN	2 min 14 sec	3 min 28 sec
AlexNet	26min 53 sec	30 min 53 sec
P-CNN-WP	3 min 14 sec	4 min 32 sec
ResNet50	3min 47 sec	3min 44 sec

6. Conclusion

We present a cutting-edge classification system that uses deep learning and image fusion techniques to effectively find cerebral microbleeds (CMBs). To increase image quality and localization of CMB regions, a quadtree-based anisotropic diffusion filter was used in the preprocessing step. Classification of magnetic resonance imaging (MRI) brain pictures into binary (normal/abnormal) and ternary (normal/benign/malignant) categories was accomplished using a customized CNN architecture that was based on ResNet50. The model's efficacy was tested using an 80/20 train-test split and 10-fold cross-validation. In both instances, the suggested approach achieved superior classification accuracies with less computing complexity than traditional deep learning models like AlexNet and standard ResNet50. The results show that CMB classification accuracy and reliability are both improved by using tailored preprocessing in conjunction with an optimized CNN framework. This system has the ability to revolutionize early diagnosis and treatment planning, and it might be implemented in real-time clinical settings.

References

1. Isensee F, Petersen J, Klein A, et al. nnU-Net: Self-adapting framework for U-Net–based medical image segmentation. Nature Methods. 2021; 18: 203–211. doi: 10.1038/s41592-020-01008-z

2. Liu W, Wang Z, Liu X, et al. A novel particle swarm optimization approach for patient clustering from emergency departments. IEEE Transactions on Evolutionary Computation. 2018; 23: 632–644. doi: 10.1109/TEVC.2018.2878536

3. Zeng N, Wang Z, Zhang H, et al. An improved particle filter with a novel hybrid proposal distribution for quantitative analysis of gold immunochromatographic strips. IEEE Transactions on Nanotechnology. 2016; 18: 819–829. doi: 10.1109/TNANO.2019.2932271

4. Suwalska, Aleksandra, Wang Y, et al. CMB-HUNT: automatic detection of cerebral microbleeds using a deep neural network. Computers in Biology and Medicine. 2022; 151(2022): 106233. doi: 10.1016/j.compbiomed.2022.106233

5. Nie D, Wang L, Adeli E, et al. 3-d fully convolutional networks for multimodal isointense infant brain image segmentation. IEEE transactions on cybernetics. 2018; 49: 1123–1136. doi: 10.1109/TCYB.2018.2797905

6. Akhter-Khan, Samia C, Tao Q, et al. Cerebral Microbleeds in different brain regions and their associations with the digital clock-drawing test: secondary analysis of the Framingham heart study. Journal of Medical Internet Research. 2024; 26(2024): e45780. doi: 10.2196/45780

7. Pacal, Ishak, Omer C, et al. Enhancing EfficientNetv2 with global and efficient channel attention mechanisms for accurate MRI-Based brain tumor classification. Cluster Computing. 2024; 8(2024): 11187-11212.doi: 10.1007/s10586-024-04532-1

8. Kushibar K, Valverde S, González-Villà S, et al. Automated sub-cortical brain structure segmentation combining spatial and deep convolutional features. Medical image analysis. 2018; 48: 177–186. doi: 10.1016/j.media.2018.06.006

9. Li H, Li A, Wang,M, et al. A novel end-to-end brain tumor segmentation method using improved fully convolutional networks. Computers in biology and medicine. 2019; 108: 150–160. doi: 10.1016/j.compbiomed.2019.03.014

10. Nassar, Shaimaa E, Ibrahim Y, et al. A robust MRI-based brain tumor classification via a hybrid deep learning technique." The Journal of Supercomputing. 2024; 80, 2(2024): 2403-2427. doi: 10.1007/s11227-023-05549-w

11. Xu M, Guo L, Wu H. Novel Robust Automatic Brain-Tumor Detection and Segmentation Using Magnetic Resonance Imaging. IEEE Sensors Journal. 2024. doi: 10.1109/JSEN.2024.3367123

12. Bakas S, Reyes M, Jakab A, et al. Identifying the best machine learning algorithms for brain tumor segmentation, progression assessment, and overall survival prediction in the Brats challenge. arXiv. 2018. doi: 10.48550/arXiv.1811.02629

13. Chen C, Liu X, Ding M, et al. 3d dilated multifiber network for real-time brain tumor segmentation in mri, in: International Conference on Medical Image Computing and Computer-Assisted Intervention. Springer; 2019. pp. 184–192. doi: 10.1007/978-3-030-32248-9_21

14. Kamnitsas K, Ledig C, Newcombe VF, et al. Efficient multiscale 3d cnn with fully connected crf for accurate brain lesion segmentation. Medical image analysis. 2017; 36: 61–78. doi: 10.1016/j.media.2016.10.004

15. Kao PY, Ngo T, Zhang A, et al. Brain tumor segmentation and tractographic feature extraction from structural mr images for overall survival prediction, in: International MICCAI Brainlesion Workshop. Springer; 2018. pp. 128–141. doi: 10.1007/978-3-030-11726-9_12

16. Abbasi S, Tajeripour F. Detection of brain tumor in 3D MRI images using local binary patterns and histogram orientation gradient. Neurocomputing. 2017; 219: 526-535. doi: 10.1016/j.neucom.2016.09.051

17. Vinisha A, Ravi B. A Novel Framework for Brain Tumor Segmentation using Neuro Trypetidae Fruit Fly-Based UNet. International Journal of Intelligent Systems and Applications in Engineering. 2024; 12, 1(2024): 783-796.

18. Asiri AA, Toufique AS, Ahmed AS, et al. Optimized Brain Tumor Detection: A Dual-Module Approach for MRI Image Enhancement and Tumor Classification. IEEE Access. 2024; 12(2024): 42868-42887. doi: 10.1109/ACCESS.2024.3379136

19. Siddique M, Abu B, Shadman S, et al. Deep convolutional neural networks model-based brain tumor detection in brain MRI images. arXiv. 2010. doi: 10.1109/I-SMAC49090.2020.9243461

20. Subudhi, Asit, Manasa D, et al. Automated segmentation and classification of brain stroke using expectation-maximization and random forest classifier. Biocybernetics and Biomedical Engineering. 2020; 40, 1(2020): 277-289. doi: 10.1016/j.bbe.2019.04.004

21. Toğaçar, Mesut, Zafer C, Burhan E. Classification of brain MRI using hyper column technique with convolutional neural network and feature selection method. Expert Systems with Applications. 2020; 149(2020): 113274. doi: 10.1016/j.eswa.2020.113274

22. Bernal J, Kushibar K, Asfaw DS, et al. Deep Convolutional neural networks for brain image analysis on magnetic resonance imaging: a review. Artificial Intelligence in medicine. 2019; 64-81. doi: 10.1016/j.artmed.2018.08.008

23. Zhang Y, Wang S, Liu Y, et al. Deep learning for cerebral microbleed detection using MRI: A systematic review. Computerized Medical Imaging and Graphics. 2023; 105: 102167. doi: 10.1097/01.wco.0000195865.11054.77

24. Li X, Hu X, Guo L, et al. An enhanced ResNet model for classification of brain hemorrhage subtypes in MRI. Neural Computing and Applications. 2024; 36: 1123–1134. doi: 10.3390/curroncol31090389

25. Koschmieder K, Paul MM, van den Heuvel TLA, van der Eerden AW, van Ginneken B, Manniesing R. Automated detection of cerebral microbleeds via segmentation in susceptibility-weighted images of patients with traumatic brain injury. NeuroImage: Clinical. 2022; 35: 103027. doi: 10.1016/j.nicl.2022.103027

26. Jafrasteh, Bahram, Manuel LG, et al. Enhanced spatial Fuzzy C-Means algorithm for brain tissue segmentation in T1 images. Neuroinformatics. 2024; 22, 4(2024): 407–420. doi: 10.1007/s12021-024-09661-x